

Article

NO-CH₄-SCR Over Core-Shell MnH-Zeolite Composites

Yixiao Li ¹, Quanhua Wang ², Ding Wang ^{1,2} and Xiaoliang Yan ^{2,*}

¹ Departments of Chemical Engineering and Chemistry, University of Kansas, Lawrence, KS 66047, USA; yixiaoli@ku.edu (Y.L.); dingwang@ku.edu (D.W.)

² College of Chemistry and Chemical Engineering, Institute of Special Chemicals, Taiyuan University of Technology, Taiyuan 030024, China; wangquanhuatyt@163.com

* Correspondence: yanxiaoliang@tyut.edu.cn or ccet6010121@163.com; Tel.: +86-351-601-8384

Received: 21 February 2019; Accepted: 21 April 2019; Published: 28 April 2019



Featured Application: Authors are encouraged to provide a concise description of the specific application or a potential application of the work. This section is not mandatory.

Abstract: Selective catalytic reduction of NO with methane (NO-CH₄-SCR) in the presence of excess oxygen was investigated over the synthesized MnH-ZZs-n zeolite composite catalysts with FAU (as core) and BEA (as shell) topologies. XRD, SEM, and NH₃-TPD technologies were employed to characterize the catalysts. It is found that the topological structure of the zeolite affected the catalytic properties and H₂O/SO₂ tolerances considerably. MnH-ZZs-n catalysts exhibited much higher NO-CH₄-SCR activity than the physical mixture catalysts with comparable relative mass content of Y and Beta zeolites, particularly the ratio of Y and Beta at the range of 0.2–0.5 than the MnH-Beta catalysts with single topology. NH₃-TPD results showed that one new type of strong acidic sites formed in H-ZZs-n and remained in MnH-ZZs-n resulted from the interaction between the Lewis and Brønsted acid sites under a particular environment. The special zeolite-zeolite structure with ion-exchanged Mn ions in the core-shell zeolite composite catalysts contributed to the novel NO-CH₄-SCR properties.

Keywords: zeolite composite; NO-CH₄-SCR; core-shell structure; FAU and BEA topology; Mn catalyst

1. Introduction

The combustion of coal, gasoline, and natural gas meets mankind's demands for energy. However, the emission of flue gas has caused severe environmental pollution, particularly NO_x (among them 90% is NO), which can not only cause acid rain and photochemical smog, but also result in the greenhouse effect. The catalytic removal of NO_x is one of the most important ways to decrease the impact of NO_x on the environment [1]. Indeed, selective catalytic reduction of NO by NH₃ (NH₃-SCR) has been put into commercial operation. However, well-known disadvantages such as storage of ammonia, costly equipment, the danger of ammonia leakage, and the possible formation of ammonium sulfates due to the reaction of SO₂ (SO₃), NH₃ and H₂O greatly restrict the widely application of this technology [2]. Thus, many researchers have made efforts to find other new reductants to substitute for NH₃. It has been found that hydrocarbons such as C₃H₆ and C₃H₈ exhibit high activity for NO reduction over many catalysts [3]. In particular, Armor's group reported that NO can be selectively reduced by CH₄ over Co ion-exchange ZSM-5 and ferrierite in the presence of excess oxygen [4]. This is of considerable interest because there are plenty of CH₄ and natural gas vehicles increasing worldwide, and CH₄ itself is a greenhouse gas with a stronger greenhouse effect than carbon dioxide. A thorough review on the state of research has been reported [5,6] in which three types of catalysts, i.e., metal oxides, loaded

metal, and zeolite loaded metal, are active for CH₄-SCR. Among them, metal-zeolite catalysts have received the greatest attention because zeolite not only has a large surface, but also acid function and high hydrothermal stability. Zeolite-based catalysts containing different metals have been reported as active materials for the selective catalytic reduction of NO_x with methane (CH₄-SCR) [4]. CO [5,7,8], Mn [6,9–11], Pd [12] etc. incorporated into ZSM-5 have been confirmed to be active sites for CH₄-SCR. On the other hand, the zeolite structure has considerably affected the CH₄-SCR reactivity. For example, ZSM-5, ferrierite, mordenite [13], and Beta [14] loaded metals exhibited high CH₄-SCR activity, while zeolite Y loaded metals are poor for the reaction. So far, almost all research has been focused only on the zeolites with single topology. In fact, zeolitic composites with different porous structure have shown the special synergic effects in catalysis [15–17]. CH₄-SCR reactivity of the catalysts based on two different zeolite structures (MOR and BEA) containing Pd and Ce was reported [18]. Compared to each individual-zeolite catalyst, the catalytic performance of the zeolite composite was significantly improved because of the synergic effects of the zeolites. In our group, a new type of zeolite composite ZZs-n with FAU and BEA topology was synthesized. CoH-Beta/Y exhibited not only high CH₄-SCR activity but also better SO₂ and H₂O tolerance than CoH-Beta. Mn-zeolite is promising for CH₄-SCR because of relatively higher tolerance to water vapor [19] than Co-zeolite with single topology. Thus, it is of considerable interest to investigate NO-CH₄-SCR over MnH-ZZs-n. It is clearly evident from the transient studies of the NO and NO + O₂ reaction that the adsorbed NO molecules must be dissociated over the partially reduced manganese sites [20]. The Mn/TiO₂ catalyst showed good phase stability during the NO_x decomposition reaction at a different temperature and exhibited a good resistance to 10 vol% H₂O and 100 ppm of SO₂ [21]. In comparison, Mn/TNT showed an impressive deNO_x potential compared to other active components in titania nanotubes [22].

In this contribution, NO-CH₄-SCR over MnH-ZZs-n is investigated. Effects of H₂O and SO₂ on the catalytic performance of MnH-ZZs-n are reported.

2. Materials and Methods

2.1. Catalyst Preparation

Zeolite composite was synthesized in the laboratory by two-step hydrothermal crystallization with sodium silicate aqueous solution (29.12% SiO₂, [OH⁻] = 2.75 mol/L), colloidal silica ([SiO₂] = 6.02 mol/L), sodium aluminate aqueous solution (31.65% Al₂O₃, [OH⁻] = 9.87 mol/L), sodium hydroxide, tetraethylammonium bromide, ammonium hydroxide aqueous solution (25% NH₃), and distilled water. The synthesis procedure was as follows: Na-Y zeolite was first synthesized in terms of the composition of (2.0–2.5) Na₂O:(4.0–6.0) SiO₂:Al₂O₃:420H₂O. The synthesis gel was autoclaved at 373 K for 24 h. Then, it was cooled down to room temperature and added to the synthesis gel of zeolite Beta under strong stirring conditions. The synthesis gel of zeolite Beta was prepared with tetraethylammonium bromide, NH₃·H₂O, colloidal silica, and sodium aluminate aqueous solution by following the procedures established by Eapen and co-workers [23]. The pH value of the above mixture was adjusted to 12.0–12.5 with concentrated H₂SO₄ acid. Finally, the resultant uniform mixture containing zeolite Y was crystallized again at 413 K for 120–160 h in a stainless-steel autoclave. The products were filtered, washed, and dried at 393 K for 8 h to obtain core-shell zeolite composite, denoted as ZZs-n (n is the ratio of zeolite Y and zeolite Beta in the composites). Some samples were further calcined at 823 K for 6 h in an air flow with a heating rate of 1 K/min. Na-Y zeolite was synthesized according to the same method, whereas Na-Beta zeolite with a Si/Al ratio of 15 was synthesized in the laboratory.

The calcined samples were first ion-exchanged with 0.1 mol·L⁻¹ of aqueous solution of NH₄NO₃ at a liquid to solid ratio of 20 mL/g. The solid products were then thoroughly washed with distilled water, dried at 383 K overnight, and finally calcined at 823 K to get H-zeolites. H-zeolites were subsequently ion-exchanged with aqueous solution of Mn(CH₃COO)₂. The obtained solid samples were washed with distilled water, dried at 383 K overnight, and calcined in air flow at a ramp of 2 K·min⁻¹ from

room temperature (RT) to 823 K and kept for three hours to obtain MnH-ZZs-n catalysts. MnNa-ZZs-n catalysts were acquired using the same process. The ion-exchange conditions and selected properties of the catalysts were listed in Table 1. With a decrease of zeolite Y in the zeolite composites, the special surface areas of the composites decreased because of a larger surface area of zeolite Y than zeolite Beta.

Table 1. Preparation catalyst and the selected physical properties.

| Catalyst | Si/Al | Ion-Exchange Condition ^a | | | | | Mn wt. % | Mn/Al | S _{BET} (m ² ·g ⁻¹) |
|---------------|-------|-------------------------------------|--------------------------|-----|-------|---|----------|-------|---|
| | | T (K) | C (mol·L ⁻¹) | L/S | t (h) | N | | | |
| MnH-Y | 2.0 | 353 | 0.01 | 20 | 24 | 3 | 2.55 | 0.12 | 576 |
| MnH-Beta | 15.0 | 353 | 0.01 | 20 | 24 | 3 | 2.12 | 0.38 | 405 |
| H-ZZs-0.5 | 12.2 | 353 | — | — | — | — | 0 | 0 | 420 |
| MnNa-ZZs-0.5 | 12.2 | 353 | 0.01 | 20 | 24 | 3 | 2.07 | 0.37 | 428 |
| MnH-ZZs-1.0 | 10.8 | 353 | 0.01 | 20 | 24 | 3 | 2.27 | 0.31 | 379 |
| MnH-ZZs-0.5 | 12.2 | 353 | 0.01 | 20 | 24 | 3 | 2.15 | 0.38 | 359 |
| MnH-ZZs-0.3 | 13.1 | 353 | 0.01 | 20 | 24 | 3 | 2.16 | 0.38 | 365 |
| MnH-ZZs-0.2 | 14.5 | 353 | 0.01 | 20 | 24 | 3 | 2.23 | 0.39 | 363 |
| MnH-ZZs-0.5-1 | 12.2 | 353 | 0.01 | 20 | 24 | 2 | 1.82 | 0.32 | 359 |
| MnH-ZZs-0.5-2 | 12.2 | 353 | 0.01 | 20 | 24 | 1 | 1.27 | 0.25 | 356 |
| MnH-ZZs-0.5-3 | 12.2 | 353 | 0.008 | 20 | 24 | 1 | 0.92 | 0.17 | 354 |

^a : T, C, L/S, t and N represent ion-exchange temperature, concentration of solution, liquid to solid ratio, ion-exchange time and times.

2.2. Catalyst Characterization

The crystalline of the catalysts was determined by using X-ray diffraction measurement (XRD; Rigaku D/max_2500V) with Cu-K α radiation. The crystallinity the zeolite composite catalysts were estimated by comparing the areas of the selected diffraction peaks of (111), (220), (311), (511) and (440) for zeolite Y, and those of (101) and (302) for zeolite Beta based on the corresponding reference samples, respectively. The credibility of this method has been proven by the linear increase in the intensity of the diffraction peaks of these two types of zeolites with increasing zeolite phase contents in the mixture of amorphous silica and zeolite. In this way, n values in the Mn-ZZs-n samples were estimated as 1.0, 0.5, 0.3, 0.2, respectively. Thus, the mechanical mixtures (designated as ZZm-n) with the corresponding amounts of MnH-Y and MnH-Beta phases were prepared for comparison. Specific surface areas of the catalysts were measured by physical adsorption/desorption of N₂ at 77 K isotherms on NOVA 1200e. The elemental composition of the catalysts was determined by atom absorption spectrum (AAS). The morphology of the catalyst was observed by using a field emission scanning electron microscope (FE-SEM S-5200).

Temperature programmed desorption of ammonia (NH₃-TPD) tests were performed on a chemical BET surface apparatus (CHEMBET 3000) equipped with a thermal conductivity detector (TCD). An 0.15 g sample was loaded into a U model quartz tube, treated at 923 K in ultra-highly purified (UHP, 99.999%) He flow for 1 h, and then cooled down to 373 K. The sample was saturated with 10% NH₃/He at 373 K and purged with UHP He flow at 373 K for 30 min. The NH₃-TPD test was conducted by heating the sample in 80 mL·min⁻¹ UHP He flowing at a rate of 10 K·min⁻¹. During the NH₃-TPD test course, a water trap was equipped between the sample and the TCD to avoid interference by water.

2.3. Catalytic Activity Measurements

The NO-CH₄-SCR test was carried out in a fixed-bed micro-reactor system consisting of a 6 mm I.D. quartz reactor tube, a temperature controller with K mode thermoelectric couple, four mass flowing controllers, and a gas chromatograph (GC 9A) equipped with a TCD. The catalyst samples were palletized, crushed, and sieved to 40~60 mesh for the catalytic tests. The 0.3 g particular catalyst was packed into the micro-reactor and pretreated in He flow (40 mL·min⁻¹) at a ramp of 1 K·min⁻¹ from room temperature to 673 K and kept for 1 h. Then, the sample was cooled down to 473~573 K and

the reaction mixture containing 2180 ppm NO, 2050 ppm CH₄, 2% O₂, balanced by He flowed through the catalyst at 75 mL·min⁻¹ (GHSV 7500 h⁻¹ by assuming the bulk density of the catalyst 0.5 g·cm⁻³).

Under oxidizing conditions, sulfur compounds end up mainly as SO₂; therefore, SO₂ was chosen as model sulfur compound. For reactions involving SO₂, a reactor with two-inlets was used to minimize contamination of the system by SO₂ exposure. SO₂/He (294 ppm) was added to the reactor via a separate inlet. The final concentration in the feed was 78 ppm. Water vapor was added to the feed using an H₂O saturator comprised of a sealed glass bubbler with a medium-pore frit immersed in distilled water. Helium (20 mL·min⁻¹) flowed through the bubbler, carrying H₂O vapor to the feed. The bubbler was placed in a constant temperature tank. Different amounts of H₂O vapor could be added to the feed by adjusting temperature of the bubbler. The gas line containing H₂O vapor was heated traced to a temperature higher than the saturation temperature. An ice-cooled H₂O condenser was incorporated downstream of the reactor before effluent gas entering gas chromatograph.

The compositions of the effluent gas were analyzed by using the GC with molecular sieve-5A column for N₂, O₂, CH₄, CO, and Porapak Q column for CO₂ and N₂O. Negligible N₂O was formed in the effluent gas. NO and NO₂ were quantified by using a flue gas analyzer (Kane May, UK). The catalytic activity was evaluated based on the NO to N₂ conversion $C_{NO} = 2 \times ([N_2]^o/[NO]^i) \times 100\%$ where $[N_2]^o$ and $[NO]^i$ represent concentration of outlet N₂ and inlet NO, respectively. CH₄ conversion C_{CH_4} was expressed as: $C_{CH_4} = (([CH_4]^i - [CH_4]^o)/[CH_4]^i) \times 100\%$, where $[CH_4]^i$ and $[CH_4]^o$ represent the concentration of CH₄ in inlet and outlet, respectively. The above experiments were repeated three times, and the data were the average of these three runs.

3. Results and Discussion

3.1. XRD Patterns of the Catalysts

Figure 1 shows the XRD patterns of MnH-ZZs-n (n = 1.0, 0.5, 0.3, 0.2), in which all diffraction peaks are assigned to the characteristics of FAU and BEA topologies, without other undetermined crystalline phases. The crystallinities of the MnH-ZZs-n catalysts are 90~95% of the parent H-ZZs-n samples, respectively, indicating the zeolite lattices were undisturbed after ion exchanging because of the mild ion-exchanged conditions and the low metal loadings.

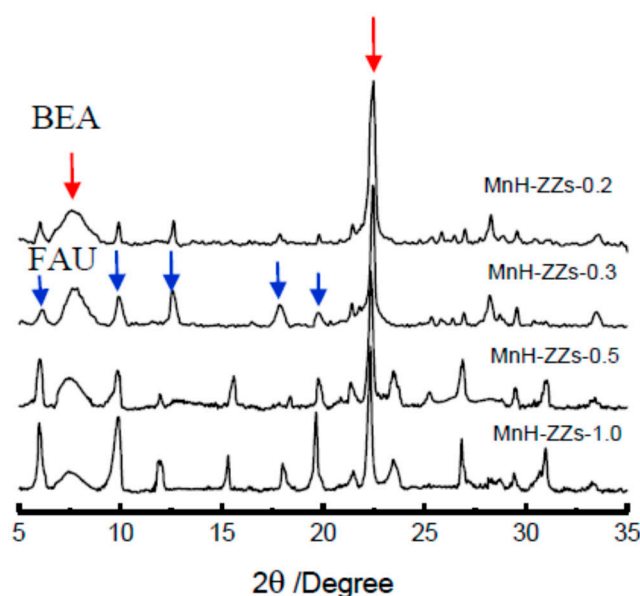


Figure 1. XRD patterns of MnH-ZZs-n (n = 1.0, 0.5, 0.3, 0.2).

FE-SEM measurements (Figure 2) show that MnH-Y prepared by the same method as that for synthesizing the ZZs-n composite is composed of typical octahedral crystals, MnH-Beta has an irregular

spherical shape. As expected, the mechanical zeolite mixture consists of two types of crystals belonging to MnH-Y and MnH-Beta without uniform distribution, and they are closed contact with each other. For the MnH-ZZs-0.5 composite sample, due to an epitaxial growth of tetragonal BEA structure around cubic FAU structure, the special octahedral crystals of zeolite Y are not easily observed because of the formation of a core-shell structure, resulting in a morphology somewhat similar to MnH-Beta. But the composite catalyst is markedly different from MnH-Y (Figure 2A) and MnH-ZZm-0.5 (Figure 2C).

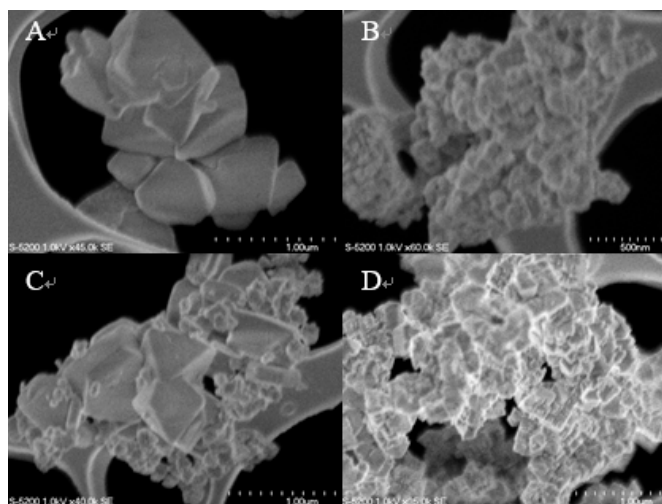


Figure 2. FE-SEM images of (A) MnH-Y, (B) MnH-Beta, (C) MnH-ZZm-0.5 and (D) MnH-ZZs-0.5.

3.2. NH_3 -TPD Results

NH_3 -TPD results H-zeolites and MnH-zeolite catalysts are shown in Figure 3. The TPD curves of the H-Y show two partially overlapping NH_3 desorption peaks at low temperature (around at 498 K and 538 K), which are attributed to desorption of NH_3 from weak acidic sites and an overlapping peak at high temperature (around at 633 K), which is attributed to the desorption of NH_3 from protonic H^+ sites. After ion-exchange with Mn cations, total amount of weak acidic sites in the catalyst increased because Mn^{2+} cations are a Lewis acid, while the amount of protonic H^+ sites decreased because they are displaced by Mn^{2+} cations. The NH_3 -TPD profile of H-Beta shows two well-resolved peaks at about 513 K and 673 K. Similar NH_3 -TPD curves are reported for the H-Beta samples with comparable Si/Al ratio [24]. The amount of protonic H^+ sites in the MnH-Beta also decreased because of ion exchange. NH_3 -TPD results of the physical mixture of H-Y+H-Beta and ZZm-0.3 are very close to the algebra sum of those of the single phase (not shown).

Worthily, the desorption peak of NH_3 in H-ZZs-0.3 from 843 K shifts to 873 K in MnH-ZZs-0.3, showed an increase in the acid strength, although the amount of the strong acidic sites decreased considerably because of the exchange of part of H^+ cations with Mn^{2+} ions (Figure 3A(c),B(c)). The formation of highly strong acid sites in the zeolite composite originated from the epitaxial growth of zeolite Beta on the zeolite Y because of an interface structure different from both zeolite Beta and Y structures. The results are supported by framework IR spectroscopies of the physical mixture of the two zeolites and the Y@Beta zeolite composite [25]. However, there is still no effective technique to ascertain the ion sites in the high silicon zeolite even with single topology. But then, the Brønsted acidity of a zeolite is also influenced by the presence of Lewis acidity. This synergy between Lewis and Brønsted acid sites resulted in an increase of the acid strength, in which the combination of Brønsted and Lewis acids can render superacids with remarkably enhanced strength [26]. In the former research on the CoH-Y/Beta catalysts, we concluded that CO ion exchange sites existed in H-Y/Beta zeolite composite in an indirect method. Mn^{2+} cations in the zeolite composite occupied the similar sites to Co^{2+} in the catalysts [25].

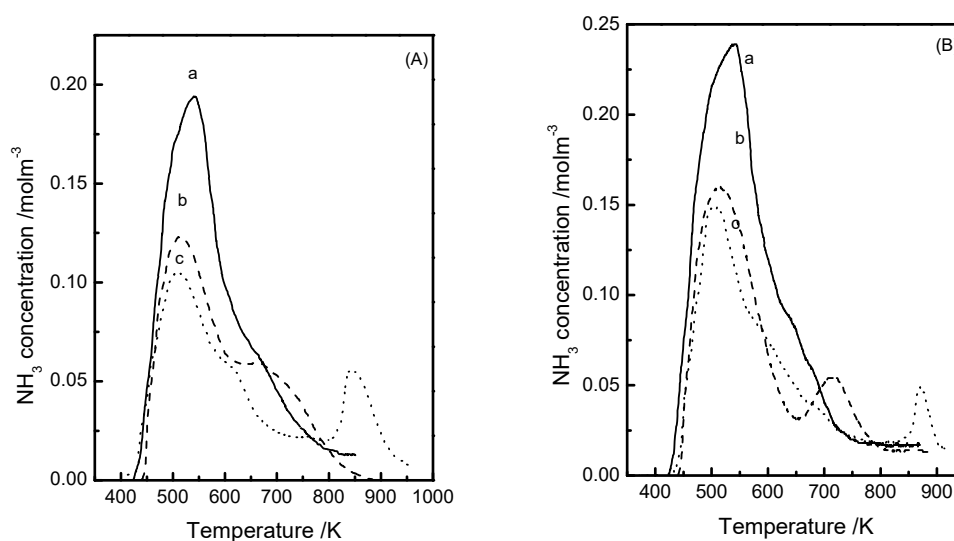


Figure 3. NH₃-TPD spectra of (A) H-zeolite a. H-Y, b. H-Beta, c. H-ZZs-0.3; (B) MnH-zeolite a. MnH-Y, b. MnH-Beta, c. MnH-ZZs-0.3.

3.3. Catalytic Activity Studies

NO-CH₄-SCR reaction results over the catalysts are summarized in Table 2. In the process, NO is converted to N₂ and CH₄ is converted to CO₂ completely. MnH-Y exhibits low NO-CH₄-SCR activity in the entire test temperature range, which is similar to that over CoH-Y. The maximal NO to N₂ conversion was 61.1% at 773 K over MnH-Beta. This is probably due to the different cation coordination and the different acidity of these two types of zeolites [8,27,28]. The cation coordination is influenced by the ligand, crystal field and topological structure of zeolites [28], whereas the acidity depends on the zeolite structure. These two factors collaborate to promote NO conversion to N₂ in NO-CH₄-SCR [27,28]. As expected, the NO to N₂ conversion over ZZm-n decreases with the content of MnH-Beta in the zeolite mixtures, and is lower than that over MnH-Beta in the entire test temperature range.

NO to N₂ conversions over MnH-ZZs-n are higher than that over ZZm-n in the entire test temperature range, although the relative content of BEA and FAU phase is comparable. Moreover, the methane conversion over MnH-ZZs-n was suppressed because of the different types of Mn²⁺ cations and the interaction with acid sites in zeolites. The maximal NO to N₂ conversion over MnH-ZZs-n catalysts has a maximum with the change of zeolite Y phase in the composites. The maximal NO to N₂ conversions are 74.6%, 77.3%, 65.8%, and 46.8%, respectively, over MnH-ZZs-n (n = 1.0, 0.5, 0.3, 0.2).

If there is no synergic effect between two zeolites in the composites, the NO to N₂ conversions over MnH-ZZs-n catalysts, such as at T = 773 K or 823 K, should be closed to those over the physical mixtures MnH-ZZm-n. Practically, a significant difference is indicated, particularly in the case of the relative contents of zeolite Y in the composites between 0.2 and 0.5. In all cases, a positive synergic effect for NO to N₂ conversion is observed over the core-shell composite catalysts [18].

To understand the effect of protonic sites in the catalysts, activity tests were performed over MnNa-ZZs-0.5 and MnH-ZZs-0.5 prepared with the same parent Na-ZZs-0.5 zeolite composite. The results in Table 2 show that NO to N₂ conversions over MnNa-ZZs-0.5 and MnH-ZZs-0.5 catalysts are comparable at a temperature below 723 K. Increasing the reaction temperature, NO-CH₄-SCR activity over MnH-ZZs-0.5 is much higher than that over MnNa-ZZs-0.5. The maximal NO to N₂ conversions are 77.3% at 823 K over MnH-ZZs-n and 55.5% over MnNa-ZZs-n at the same temperature. It is well known that the acidic OHs in zeolites are active in adsorbing and perturbing hydrocarbon molecules, and nitrogen oxides as well [29], the protonic sites promoted NO-CH₄-SCR. Obviously the synergistic effect between the metal and protonic sites of zeolite is reflected only at a higher temperature in the reaction system.

Table 2. CH₄-SCR activity over MnH-ZZs-n, MnH-Y, MnH-Beta and physical mixture samples in the absence of H₂O and SO₂.

| Sample | NO Conversion to N ₂ (CH ₄ Conversion to CO ₂) (%) | | | | | | | |
|--------------|--|----------------------------|------------------------------|------------------------------|------------------------------|-------------------------------|-------------------------------|-------------------------------|
| | 573 K | 623 K | 673 K | 723 K | 773 K | 823 K | 873 K | 923 K |
| MnH-ZZs-1.0 | 3.4 ± 0.14 (1.3 ± 0.11) | 5.6 ± 0.23 (3.2 ± 0.21) | 20.5 ± 1.01 (15.5 ± 0.78) | 47.6 ± 2.00 (39.8 ± 1.99) | 69.0 ± 3.01 (66.4 ± 3.60) | 74.6 ± 3.56 (84.4 ± 5.49) | 71.8 ± 3.20 (98.4 ± 6.00) | 66.5 ± 3.01 (100.0 ± 0.36) |
| MnH-ZZs-0.5 | 2.8 ± 0.13 (1.6 ± 0.11) | 5.4 ± 0.26 (2.8 ± 0.18) | 21.6 ± 1.00 (14.8 ± 0.74) | 54.8 ± 2.61 (42.4 ± 2.10) | 75.5 ± 3.11 (73.2 ± 4.06) | 77.3 ± 3.66 (85.4 ± 5.25) | 72.8 ± 2.90 (99.4 ± 6.01) | 68.7 ± 3.00 (100.0 ± 0.50) |
| MnH-ZZs-0.3 | 2.5 ± 0.11 (1.4 ± 0.09) | 4.8 ± 0.22 (3.1 ± 0.20) | 17.5 ± 0.81 (11.4 ± 0.56) | 36.5 ± 1.62 (26.2 ± 1.29) | 57.8 ± 2.25 (58.5 ± 0.76) | 65.8 ± 3.29 (80.2 ± 5.10) | 61.6 ± 2.10 (98.2 ± 5.95) | 54.4 ± 2.45 (100.0 ± 0.42) |
| MnH-ZZs-0.2 | 2.1 ± 0.10 (1.2 ± 0.08) | 3.6 ± 0.16 (3.0 ± 0.19) | 10.5 ± 0.49 (8.7 ± 0.43) | 25.5 ± 1.05 (22.6 ± 1.10) | 41.8 ± 1.80 (50.7 ± 2.82) | 46.8 ± 2.36 (73.6 ± 4.66) | 47.4 ± 1.01 (93.2 ± 7.50) | 43.4 ± 1.98 (100.0 ± 0.36) |
| H-ZZs-0.5 | 0.9 ± 0.09 (0.1 ± 0.01) | 1.5 ± 0.09 (0.2 ± 0.02) | 3.7 ± 0.15 (1.6 ± 0.10) | 10.8 ± 0.45 (6.2 ± 0.70) | 17.3 ± 0.71 (14.2 ± 0.80) | 20.5 ± 1.03 (25.1 ± 1.93) | 22.1 ± 0.53 (30.2 ± 2.51) | 23.9 ± 1.01 (34.8 ± 1.50) |
| MnH-Y | 2.5 ± 0.11 (2.7 ± 0.19) | 3.9 ± 0.18 (3.1 ± 0.20) | 4.7 ± 0.19 (2.8 ± 0.13) | 5.7 ± 0.25 (2.9 ± 0.32) | 6.4 ± 0.30 (7.3 ± 0.45) | 6.7 ± 0.33 (11.4 ± 1.71) | 10.6 ± 2.21 (17.6 ± 1.47) | 11.9 ± 0.53 (23.9 ± 1.00) |
| MnH-Beta | 3.6 ± 0.15 (2.4 ± 0.17) | 7.0 ± 0.20 (4.4 ± 0.27) | 19.2 ± 0.82 (14.7 ± 0.70) | 47.4 ± 2.01 (46.2 ± 2.15) | 61.1 ± 3.00 (84.2 ± 4.10) | 56.3 ± 2.56 (100.0 ± 0.60) | 49.7 ± 2.30 (100.0 ± 0.34) | - |
| MnNa-ZZs-0.5 | 2.8 ± 0.12 (3.1 ± 0.21) | 4.3 ± 0.20 (4.6 ± 0.28) | 21.1 ± 0.76 (18.6 ± 0.90) | 49.9 ± 2.12 (44.7 ± 2.20) | 60.1 ± 2.90 (86.4 ± 0.10) | 55.4 ± 2.61 (99.8 ± 5.99) | 41.2 ± 1.98 (100.0 ± 0.46) | - |
| MnH-ZZm-1.0 | 4.0 ± 0.14 (1.3 ± 0.09) | 5.8 ± 0.19 (4.6 ± 0.27) | 16.8 ± 0.75 (17.5 ± 0.87) | 46.2 ± 2.00 (36.4 ± 1.65) | 56.8 ± 2.52 (70.8 ± 2.85) | 56.1 ± 2.56 (98.5 ± 5.85) | 56.4 ± 2.41 (100.0 ± 0.35) | - |
| MnH-ZZm-0.5 | 3.1 ± 0.14 (1.3 ± 0.09) | 4.9 ± 0.24 (2.2 ± 0.14) | 12.7 ± 0.59 (16.6 ± 0.82) | 35.1 ± 1.56 (28.6 ± 1.39) | 55.6 ± 2.45 (67.9 ± 2.80) | 56.6 ± 2.57 (93.2 ± 6.56) | 51.7 ± 2.36 (100.0 ± 0.42) | - |
| MnH-ZZm-0.3 | 2.4 ± 0.14 (1.2 ± 0.10) | 3.6 ± 0.22 (2.1 ± 0.13) | 11.7 ± 0.50 (12.1 ± 0.61) | 26.1 ± 1.10 (2.35 ± 0.10) | 43.7 ± 1.95 (45.3 ± 2.25) | 51.1 ± 2.42 (81.5 ± 5.25) | 50.4 ± 2.35 (95.8 ± 5.10) | 41.0 ± 1.90 (100.0 ± 0.45) |
| MnH-ZZm-0.2 | 2.4 ± 0.14 (1.2 ± 0.09) | 3.8 ± 0.12 (1.9 ± 0.12) | 5.9 ± 0.21 (6.4 ± 0.32) | 17.7 ± 0.71 (14.8 ± 1.35) | 33.2 ± 1.59 (29.5 ± 1.60) | 43.7 ± 2.19 (58.6 ± 4.20) | 49.1 ± 2.32 (86.0 ± 4.98) | 47.4 ± 2.10 (99.5 ± 0.14) |

Reactant composition in the inlet: NO 2180 ppm, CH₄ 2050 ppm, O₂ 2%; GHSV 7500 h⁻¹.

Table 3 showed the effect of Mn content in the catalysts on the NO-CH₄-SCR activity. The NO-CH₄-SCR activity increases considerably over the catalysts incorporated with Mn loadings. However, MnNa-ZZs-n and MnH-ZZs-n exhibited similar activity at a temperature lower than 673 K, indicating the ion-exchange Mn in the zeolite composites play a key role in NO-CH₄-SCR. As mentioned above, the synergic effect of metal ions and protonic sites resulted in much higher NO-CH₄-SCR activity over MnH-ZZs-n than MnNa-ZZs-n at a high reaction temperature. The transient response analysis and in situ FT-IR studies, by exploring the surface interactions of isotopic labeled reactants, showed that the reaction follows a Mars-van-Krevelen-like mechanism through the formation of nitrosamide and azoxy intermediates [30]. The normalized NO_x conversions with respect to a different carrier (support) as a function of surface active sites indicating that the promoted or isolated Mn⁴⁺ and Ce³⁺ species located over the surface of TiO₂ are responsible for the high deNO_x efficiency over Mn-Ce/TiO₂ (Hk) catalyst [31]. So far, there still remain questions about the reaction mechanism and the potential intermediate species over the Mn-based catalysts [30]. It can be concluded that Mn²⁺ cations in the ion-exchanged zeolites are active sites and acid sites of zeolite play a minor role in the CH₄-SCR of NO to N₂ at low reaction temperature; with increase of the reaction temperature, the synergic effects of metal ions and protonic sites are the key factors for improving the reaction [13].

As a result, the properties of the ZZs zeolite composites are completely different from the physical mixtures of zeolites ZZm in the reaction, the introduction of the protons into zeolites increases the conversion of NO to N₂, and but decreases the conversion of CH₄ to CO₂ under the same reaction conditions. The introduction of Mn²⁺ cations into zeolites greatly increases the conversions of NO to N₂ and CH₄ to CO₂. The appearance of the strong acid sites partially increases the activity of the catalysts at a low temperature.

Table 3. Effect of the Mn content in the MnH-ZZs-n on the catalytic activity.

| Sample | NO Conversion to N ₂ (CH ₄ Conversion to CO ₂) (%) | | | | | | | |
|---------------|--|----------------------------|------------------------------|------------------------------|------------------------------|------------------------------|-------------------------------|-------------------------------|
| | 573 K | 623 K | 673 K | 723 K | 773 K | 823 K | 873 K | 923 K |
| MnNa-ZZs-0.5 | 2.8 ± 0.12 (3.1 ± 0.21) | 4.3 ± 0.20 (4.6 ± 0.28) | 21.1 ± 0.76 (18.6 ± 0.90) | 49.9 ± 2.12 (44.7 ± 2.20) | 60.1 ± 2.90 (86.4 ± 0.10) | 55.4 ± 2.61 (99.8 ± 5.99) | 41.2 ± 1.98 (100.0 ± 0.46) | - |
| MnH-ZZs-0.5 | 2.8 ± 0.13 (1.6 ± 0.11) | 5.4 ± 0.26 (2.8 ± 0.18) | 21.6 ± 1.00 (14.8 ± 0.74) | 54.8 ± 2.61 (42.4 ± 2.10) | 75.5 ± 3.11 (73.2 ± 4.06) | 77.3 ± 3.66 (85.4 ± 5.25) | 72.8 ± 2.90 (99.4 ± 6.01) | 68.7 ± 3.00 (100.0 ± 0.50) |
| MnH-ZZs-0.5-1 | 2.4 ± 0.18 (1.2 ± 0.10) | 4.2 ± 1.13 (3.6 ± 0.80) | 16.9 ± 1.13 (11.6 ± 0.81) | 43.4 ± 2.71 (31.9 ± 2.01) | 55.1 ± 3.30 (63.3 ± 3.50) | 59.8 ± 3.60 (81.4 ± 5.00) | 62.6 ± 3.21 (99.8 ± 5.52) | 56.9 ± 3.01 (100.0 ± 0.51) |
| MnH-ZZs-0.5-2 | 2.3 ± 0.16 (1.3 ± 0.11) | 4.5 ± 0.93 (3.5 ± 0.75) | 13.9 ± 0.95 (10.7 ± 0.75) | 33.2 ± 2.10 (26.5 ± 1.81) | 48.1 ± 2.90 (47.6 ± 2.81) | 53.9 ± 3.45 (79.7 ± 4.95) | 55.3 ± 2.95 (91.2 ± 5.01) | 50.6 ± 2.61 (100.0 ± 0.46) |
| MnH-ZZs-0.5-3 | 2.5 ± 0.17 (1.1 ± 0.09) | 3.9 ± 0.75 (3.3 ± 0.65) | 10.9 ± 0.80 (8.3 ± 0.66) | 26.6 ± 1.72 (24.7 ± 1.71) | 38.1 ± 2.15 (36.2 ± 2.16) | 43.2 ± 2.81 (65.7 ± 4.01) | 45.6 ± 2.60 (85.4 ± 4.80) | 45.2 ± 2.41 (100.0 ± 0.50) |
| H-ZZs-0.5 | 0.9 ± 0.09 (0.1 ± 0.01) | 1.5 ± 0.09 (0.2 ± 0.02) | 3.7 ± 0.15 (1.6 ± 0.10) | 10.8 ± 0.45 (6.2 ± 0.70) | 17.3 ± 0.71 (14.2 ± 0.80) | 20.5 ± 1.03 (25.1 ± 1.93) | 22.1 ± 0.53 (30.2 ± 2.51) | 23.9 ± 1.01 (34.8 ± 1.50) |

Reactant composition in the inlet: NO 2180 ppm, CH₄ 2050 ppm, O₂ 2%; GHSV 7500 h⁻¹.

3.4. The Effects of H₂O and SO₂ on NO-CH₄-SCR Activity

During the combustion of the fuel, the existence of H₂O and SO₂ in the exhaust is inevitable. Indeed, the existence of H₂O and SO₂ greatly suppressed CH₄-SCR catalytic activity of the Co-zeolite catalysts [5]. Mn-ZSM-5 exhibited better H₂O tolerance than Co-ZSM-5 for CH₄-SCR [11]. Thus, it is of considerable interest to study H₂O and SO₂ tolerance of the MnH-ZZs-n for CH₄-SCR. Figure 4 shows the NO-CH₄-SCR activity over MnH-ZZs-0.5 and MnH-Beta at 773 K in the presence of H₂O or/and SO₂.

As shown in Figure 4A, addition of 2.5% (*v/v*) water vapor, NO to N₂ conversion over MnH-ZZs-0.5 decreases from 75.2% a stable level 51.2% in about 3 h, while the CH₄ conversion decreases from 73.3% to 48.1%. In the same condition, NO to N₂ conversion over MnH-Beta decreases from 61.1% to 36.0% from 30 min to 200 min, and the conversion of CH₄ decreases from 84.2% to 58.9%. As the water is removed, the CH₄-SCR activity almost recovers to the original extent, which indicated that the deactivation caused by the water is reversible. The decrease in the activity in the presence of water vapor may be due to the competence of H₂O with NO for interacting with Mn²⁺ ions to form hydrated

species. The adsorption of H_2O on the catalysts is physical and/or weak-chemical, and there are no strong chemical bonds formed between H_2O and active sites on the surface of the catalysts. In other words, the Mn catalysts have a good resistance to H_2O [21,32]. Notably, the introducing of water vapor did not damage the topologic structure of the zeolites to remove the framework Al and decrease Brönsted acid sites even at high temperatures because of the special zeolite-zeolite structure with high hydrothermal ability.

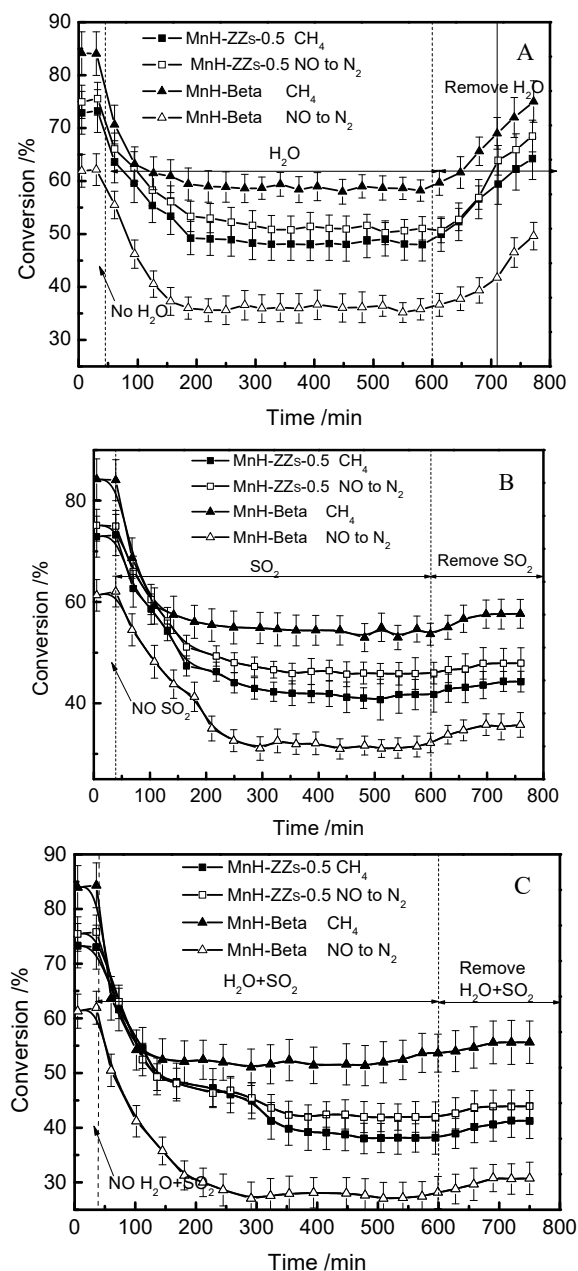


Figure 4. Effect of (A) water vapor, (B) SO_2 and (C) H_2O+SO_2 on the CH_4 -SCR activity over MnH-ZZs-0.5 and MnH-Beta. Reaction condition: NO 2180 ppm, CH_4 2050 ppm, O_2 2%, H_2O 2%/SO₂ 78 ppm GHSV 7500 h⁻¹.

In Figure 4B, in the dry condition, addition of 78 ppm SO_2 made NO conversion to N_2 over MnH-ZZs-0.5 decreases from 75.2% to a stable level 46.4% in about 4 h and CH_4 conversion drops from 73.2% to 41.4%. In the same condition, NO to N_2 conversion changes from 61.3% to a stable level 31.2% and CH_4 conversion alters from 84.4% to 55.2%. As SO_2 is removed, the CH_4 -SCR activity is

only partially recovered, indicating that deactivation caused by SO₂ is irreversible. However, for the selective reduction of NO_x to N₂ with NH₃ in the presence of an excess of oxygen, sulfur dioxide with a broad temperature window indicated without sacrificing too much of the efficiency [30], on this point, complexing ability of NH₃ with metal or metal ions is much stronger than that of SO₂, which itself has a strong interaction with Mn²⁺ and formed chemical bond in the CH₄-SCR reaction system.

In Figure 4C, as 2.5% H₂O and 78 ppm SO₂ are introduced at the same time, NO to N₂ conversion over MnH-ZZs-n decreases from 75.3% to 44.1% and reaches to level off in about 4 h and CH₄ conversion from 72.9% to 42.4%. In the same condition, NO to N₂ conversion over MnH-Beta decreases from 61.2% to 27.2% and to level off in about 4 h, CH₄ conversion from 83.9% to 52.4%. As H₂O and SO₂ are removed, the CH₄-SCR activity recovers only a little, which indicates that the deactivation caused by the co-existence of H₂O and SO₂ is irreversible because of the presence of SO₂ in the reaction system.

4. Conclusions

MnH-ZZs-n core-shell zeolite composite catalysts used in NO-CH₄-SCR showed the higher activity than the physical mixtures MnH-ZZm-n, single phase FAU, or BEA zeolite. One new type of strong acidic site existed in H-ZZs-n and changed the NO-CH₄-SCR reactivity of MnH-MMs-n. Mn²⁺ cations, key active centres for NO-CH₄-SCR at low temperature, and protonic acid sites increased the conversion of NO at a high temperature. The special structure properties of zeolite composite resulted in the high reaction activity of MnH-ZZs-n in NO-CH₄-SCR. The strong H₂O tolerance of the catalyst in NO-CH₄-SCR resulted from the new topology structure of zeolite composite and weak SO₂ tolerance from the interaction with Mn cations.

Author Contributions: Conceptualization, X.Y. and Y.L.; methodology, X.Y.; validation, Y.L., X.Y. and Q.W.; formal analysis, D.W.; investigation, Y.L. and Q.W.; resources, X.Y.; data curation, D.W.; writing—original draft preparation, Q.W. and Y.L.; writing—review and editing, Y.L.; visualization, D.W.; supervision, X.Y.; project administration, X.Y.

Acknowledgments: This work was supported by Shanxi Provincial Key Innovative Research Team in Science and Technology (No. 2014131006).

Conflicts of Interest: The authors declare no conflict of interest.

References

1. Teng, Z.; Zhang, H.; Huang, S.; Li, N.; Zhou, Q. Experimental study on reduction of NO by CH₄ over La_{0.8}Sr_{0.2}MnO₃/α-Al₂O₃ in excess of O₂. *J. Taiwan Inst. Chem. Eng.* **2018**, *87*, 204–210. [[CrossRef](#)]
2. Busca, G.; Lietti, L.; Ramis, G.; Berti, F. Chemical and mechanistic aspects of the selective catalytic reduction of NO_x by ammonia over oxide catalysts: A review. *Appl. Catal. B Environ.* **1998**, *18*, 1–36. [[CrossRef](#)]
3. Rottländer, C.; Andorf, R.; Plog, C.; Krutzsch, B.; Baerns, M. Selective NO reduction by propane and propene over a Pt/ZSM-5 catalyst: A transient study of the reaction mechanism. *Appl. Catal. B Environ.* **1996**, *11*, 49–63. [[CrossRef](#)]
4. Mendes, A.N.; Zholobenko, V.L.; Thibault-Starzyk, F.; Da Costa, P.; Henriques, C. On the enhancing effect of Ce in Pd-MOR catalysts for NO_x CH₄-SCR: A structure-reactivity study. *Appl. Catal. B Environ.* **2016**, *195*, 121–131. [[CrossRef](#)]
5. Lónyi, F.; Solt, H.E.; Vályon, J.; Boix, A.; Gutierrez, L.B. The activation of NO and CH₄ for NO-SCR reaction over In- and Co-containing H-ZSM-5 catalysts. *J. Mol. Catal. A Chem.* **2011**, *345*, 75–80. [[CrossRef](#)]
6. Traa, Y.; Burger, B.; Weitkamp, J. Zeolite-based materials for the selective catalytic reduction of NO_x with hydrocarbons. *Microporous Mesoporous Mater.* **1999**, *30*, 3–41. [[CrossRef](#)]
7. Dědeček, J.; Čapek, L.; Kaucký, D.; Sobalík, Z.; Wichterlová, B. Siting and Distribution of the Co Ions in Beta zeolite: A UV-Vis-NIR and FTIR study. *J. Catal.* **2002**, *211*, 198–207. [[CrossRef](#)]
8. Resini, C.; Montanari, T.; Nappi, L.; Bagnasco, G.; Turco, M.; Busca, G.; Bregani, F.; Notaro, M.; Rocchini, G. Selective catalytic reduction of NO_x by methane over Co-H-MFI and Co-H-FER zeolite catalysts: Characterisation and catalytic activity. *J. Catal.* **2003**, *214*, 179–190. [[CrossRef](#)]

9. Aylor, A.W.; Lobree, L.J.; Reimer, J.A.; Bell, A.J. NO Adsorption, desorption, and reduction by CH₄ over Mn-ZSM-5. *J. Catal.* **1997**, *170*, 390–401. [[CrossRef](#)]
10. Campa, M.C.; Pietrogioiacomi, D.; Tuti, S.; Ferraris, G.; Indovina, V. The selective catalytic reduction of NO_x with CH₄ on Mn-ZSM₅: A comparison with Co-ZSM₅ and Cu-ZSM₅. *Appl. Catal. B Environ.* **1998**, *18*, 151–162. [[CrossRef](#)]
11. Sun, Q.; Sachtler, W.M.H. Mn/MFI catalyzed reduction of NO_x with alkanes. *Appl. Catal. B Environ.* **2003**, *42*, 393–401. [[CrossRef](#)]
12. Costilla, I.O.; Sanchez, M.D.; Volpe, M.A.; Gigolaa, C.E. Ce effect on the selective catalytic reduction of NO with CH₄ on Pd-mordenite in the presence of O₂ and H₂O. *Catal. Today* **2011**, *172*, 84–89. [[CrossRef](#)]
13. Campa, M.C.; Pietrogioiacomi, D.; Occhiuzzi, M. The simultaneous selective catalytic reduction of N₂O and NO_x with CH₄ on Co- and Ni-exchanged mordenite. *Appl. Catal. B Environ.* **2015**, *168*, 293–302. [[CrossRef](#)]
14. Pan, H.; Jian, Y.; Yu, Y.; He, C.; Shen, Z.; Liu, H. Regeneration and sulfur poisoning behavior of In/H-BEA catalyst for NO_x reduction by CH₄. *Appl. Surf. Sci.* **2017**, *401*, 120–126. [[CrossRef](#)]
15. Guo, W.; Huang, L.; Deng, P.; Xue, Z.; Li, Q. Characterization of Beta/MCM-41 composite molecular sieve compared with the mechanical mixture. *Microporous Mesoporous Mater.* **2001**, *44*, 427–434. [[CrossRef](#)]
16. Liu, H.; Bao, X.; Wei, W.; Shi, G. Synthesis and characterization of kaolin/NaY/MCM-41 composites. *Microporous Mesoporous Mater.* **2003**, *66*, 117–125. [[CrossRef](#)]
17. Ooi, Y.S.; Zakaria, R.; Mohamed, A.R.; Bhatia, S. Synthesis of composite material MCM-41/Beta and its catalytic performance in waste used palm oil cracking. *Appl. Catal. A Gen.* **2004**, *274*, 15–23. [[CrossRef](#)]
18. Mendes, A.N.; Matynia, A.; Toullec, A.; Capela, S.; Ribeiro, M.F.; Henriques, C.; Costa, P.D. Potential synergic effect between MOR and BEA zeolites in NO_x SCR with methane: A dual bed design approach. *Appl. Catal. A Gen.* **2015**, *506*, 246–253. [[CrossRef](#)]
19. Li, Y.; Battavio, P.J.; Armor, J.N. Effect of water vapor on the selective reduction of NO by methane over cobalt-exchanged ZSM-5. *J. Catal.* **1993**, *142*, 561–571. [[CrossRef](#)]
20. Boningari, T.; Pavani, S.M.; Ettireddy, P.R.; Chuang, S.S.C.; Smirniotis, P.G. Mechanistic investigations on NO reduction with CO over Mn/TiO₂ catalyst at low temperatures. *Mol. Catal.* **2018**, *451*, 33–42. [[CrossRef](#)]
21. Damma, D.; Boningari, T.; Ettireddy, P.R.; Reddy, B.M.; Smirniotis, P.G. Direct Decomposition of NO_x over TiO₂ Supported transition metal oxides at low temperatures. *Ind. Eng. Chem. Res.* **2018**, *57*, 16615–16621. [[CrossRef](#)]
22. Boningari, T.; Pappas, D.K.; Smirniotis, P.G. Metal oxide-confined interweaved titania nanotubes M/TNT (M = Mn, Cu, Ce, Fe, V, Cr, and Co) for the selective catalytic reduction of NO_x in the presence of excess oxygen. *J. Catal.* **2018**, *365*, 320–333. [[CrossRef](#)]
23. Eapen, M.J.; Reddy, K.S.N.; Shiralkar, V.P. Hydrothermal crystallization of zeolite beta using tetraethylammonium bromide. *Zeolites* **1994**, *14*, 295–302. [[CrossRef](#)]
24. Miyamoto, Y.; Katada, N.; Niwa, M. Acidity of β zeolite with different Si/Al₂ ratio as measured by temperature programmed desorption of ammonia. *Microporous Mesoporous Mater.* **2000**, *40*, 271–281. [[CrossRef](#)]
25. Zhang, J.; Fan, W.; Liu, Y.; Li, R. Synthesis and catalytic property of a Co²⁺-exchanged Beta/Y composite for the selective catalytic reduction of NO by CH₄ in the presence of excess oxygen. *Appl. Catal. B Environ.* **2007**, *76*, 174–184. [[CrossRef](#)]
26. Primo, A.; Garcia, H. Zeolites as catalysts in oil refining. *Chem. Soc. Rev.* **2014**, *43*, 7548–7561. [[CrossRef](#)]
27. Kaucký, D.; Vondrovà, A.; Dědčec, J.; Wichterlová, B. Activity of Co ion sites in ZSM-5, Ferrierite, and Mordenite in selective catalytic reduction of NO with methane. *J. Catal.* **2000**, *194*, 318–329. [[CrossRef](#)]
28. Armor, J.N. Catalytic reduction of nitrogen oxides with methane in the presence of excess oxygen: A review. *Catal. Today* **1995**, *26*, 147–158. [[CrossRef](#)]
29. Armadori, T.; Trombetta, M.; Gutierrez, A.A.; Ramirez, S.J.; Busca, G. FTIR study of the interaction of some branched aliphatic molecules with the external and internal sites of H-ZSM5 zeolite. *Phys. Chem. Chem. Phys.* **2000**, *2*, 3341–3348. [[CrossRef](#)]
30. Boningari, T.; Smirniotis, P.G. Impact of nitrogen oxides on the environment and human health: Mn-based materials for the NO_x abatement. *Curr. Opin. Chem. Eng.* **2016**, *13*, 133–141. [[CrossRef](#)]

31. Boningari, T.; Ettireddy, P.R.; Somogyvari, A.; Liu, Y.; Vorontsov, A.; McDonald, C.A.; Smirniotis, P.G. Influence of elevated surface texture hydrated titania on Ce-doped Mn/TiO₂ catalysts for the low-temperature SCR of NO_x under oxygen-rich conditions. *J. Catal.* **2015**, *325*, 145–155. [[CrossRef](#)]
32. Ciambelli, P.; Sannino, D.; Palo, E.; Ruggiero, A. Improved stability of Co-Ferrierite catalyst by Mn in dry–wet cycles of lean CH₄-SCR of NO_x. *Top. Catal.* **2007**, *42*, 177–181. [[CrossRef](#)]



© 2019 by the authors. Licensee MDPI, Basel, Switzerland. This article is an open access article distributed under the terms and conditions of the Creative Commons Attribution (CC BY) license (<http://creativecommons.org/licenses/by/4.0/>).